Al-Rafidain Journal of Engineering Sciences

Journal homepage https://rjes.iq/index.php/rjes

ISSN 3005-3153 (Online)

Numerical Investigation of Advanced Composite Materials for Enhanced Structural Performance and Aerodynamic Efficiency of UAV Wings

Adian Waleed Ismail[1] and Yaser Alaiwi[2]

[1,2] Department of Mechanical Engineering, Altinbas University, Istanbul 34217, Turkey

ARTICLE INFO

Article history:
Received xxxx
Revised xxxx,
Accepted xxxx,
Available online xxxx

Keywords:
Fluid-Structure Interaction (FSI)
Composite Materials
Unmanned aerial vehicle
Computational Fluid Dynamics (CFD)

ABSTRACT

In this research, the deficiencies in structural performance and aerodynamic performance of UAV wings fabricated with conventional materials have been investigated to identify how composite material can improve them. A quantitative study using CFD, FSI, and modal analysis is used to evaluate the AAI Shadow-200 RQ-7 UAV wings performance. With SOLIDWORKS for the geometry of the structures and ANSYS for the simulations, the performance of Epoxy Carbon UD Prepreg and Epoxy/glass fiber UD prepreg QI composites are compared to that of the conventional aluminum. The results reveal that the use of Epoxy/glass fiber UD prepreg QI offers the best safety factor, least deformation, and a greatly enhanced load carrying capacity. This research has added significant knowledge into the improvement of UAV wing design, the enhancement of the use of composite material in aerospace engineering, and has given a sound framework for the design of the next generation UAVs.

1. Introduction

Aircraft systems which operate without a human pilot onboard, and are remotely controlled or fly autonomously using on board sensors and GPS [1]. Since the early 1900s, UAV technology has changed from being experimental military tools to the versatile platforms used in agriculture, in disaster response, in military operations, and for civilian applications [2]. Traditional practices in different areas have been revolutionized by UAVs. As agriculture, they supply intricate soil analysis, crop health assessment, precise administration of treatments and effective management of irrigation systems. UAVs are used in military operations for surveillance, air strikes, bomb identification and to maintain security to reduce human risk and enhance mission efficiency. Photography, delivery, disaster rescue, archaeological surveys, geographic mapping, health monitoring, livestock surveillance, safety inspections, and atmospheric research are some of their civilian uses [3]. UAVs have a wide range of applications and can perform tasks which are risky, difficult or time consuming for human, and play a pivotal role in the technological advancement and usefulness of the applications in various domains.

Many studies have been carried out in the field of UAV design and optimization to solve different problems and to enhance the performance of the aircraft. Previous study [4] studied the design and aerodynamic problems of a high altitude, fixed wing mini-UAV, which highlighted the significance of airfoil selection and taking into account lower air density and temperature for high altitude flights, and it was

Corresponding author E-mail address: 223723165@ogr.altinbas.edu.tr
https://doi.org/10.61268/abx7bw28
This work is an open-access article distributed under a CC BY license (Creative Commons Attribution 4.0 International) under https://creativecommons.org/licenses/by-nc-sa/4.0/

shown that the UAV worked unstable when used in conditions other than it is designed to flight. Another study [5] optimized the structural design of fixed wing UAV's wing with a lightweight beam type design to improve the aerodynamic efficiency of the wing, producing a design applicable to the development of more efficient and longer flying UAVs. In a related study [6], the one way fluid material interaction on a plunging NACA 2412 modelled UAV wing, was studied, which revealed significant changes in wing deflection from 30 60 percent at different Reynolds numbers and angles of attack, demonstrating the significance of including FSI analysis in UAV wing design. In addition, a study [7] examined how composite materials could be used to reconfigure and analyze a tail sitter (VTOL) UAV wing, resulting in a 44.17% weight reduction and better performance than for aluminum wings. This is built upon by a subsequent study [8] using FSI simulations to analyze the aerodynamic behavior and structural responses of composite laminate wing skins, demonstrating the benefits of honeycomb structures to increase UAV wing durability and aerodynamic performance. A fixed wing UAV development and manufacturing process was studied in another comprehensive study [9], using computational tools and numerical analyses to strike a balance between weight and durability. A study [10] extended beyond fixed wing designs to design a computational framework to analyze FSI effects in passive feathering and cambering of flapping insect wings and provides valuable data for the design and optimization of bioinspired flapping wing systems. In a study, the effect of camber morphing on aeroelastic and aerodynamic performance of wings was also investigated [11] presents a new method for trailing edge deformation implementation based on an innovative shape memory alloy actuator showing that downward deflection of the trailing edge led to increased lift. A second study [13] investigated the structural analysis of UAV wings subject to wind gust using FSI analysis which showed that the maximum stress was still far below the critical value even under gust conditions. A study [14] developed a unique FSI environment to investigate the aerodynamic performance of flapping wings, by combining high fidelity fluid dynamics and structural mechanics simulations, and provided some insights for the design of more effective FWMAVs exploiting the aerodynamic benefits of flexible wings.

The application of advanced composite materials to enhance the structural performance and aerodynamic efficiency of the AAI Shadow-200 RQ-7 UAV wing has research gaps. However, there are no complete comparative analyses of structural, aerodynamic, and vibrational properties of the UAV wings made from aluminum alloys and advanced composites like Epoxy Carbon UD Prepreg and Epoxy/glass fiber UD prepreg QI in current literature. Current data is insufficient to determine the optimal composite configuration that enhances the wing performance and safety of the UAV under different loading conditions. Furthermore, the use of computational fluid dynamics (CFD), fluid structure interaction (FSI), and modal analysis in conjunction to evaluate the potential advantages of composite materials on UAV wing structures is rarely found in the literature, and there is a demand for further investigation of the long-term durability and environmental effects on these materials.

By building on previous work, our study enhances the understanding of UAV wing design by combining structural and aerodynamic simulations through CFD, FSI, and modal analysis while employing composite material to overcome certain performance constraints associated with aluminum wings. In contrast to Sharma et al.'s work [4], which discusses airfoil selection for high-altitude UAVs, our study includes an assessment of material impact under different aerodynamic loads. Rather than focusing on the wing structure as Yu [5] did without performing extensive analysis on the vibration of the structure, we carry out modal analysis to avoid any vibration or structural failure when in operation as a UAV.

Moreover, Narayanan et al. [6] and Basri et al. [8] investigated the fluid material

interaction, but the current study advances them by employing a two way FSI with composite material which possess a higher safety factor and low deformation. In comparison to the recent work of El Adawy et al. [9] which emphasizes on lightweight design, our study remarkably finds that Epoxy/glass fiber UD prepreg QI composite is better for safety and performance.

The novelty of our work is in combining CFD, FSI, and modal analysis in one paper, which is currently missing in the literature, in terms of the assessment of composite materials for UAV wings. The current paper offers significant findings on the best design of UAVs and lays a strong background for the subsequent research on durability and environmental resilience.

In this research, the potential of advanced composite materials, namely Epoxy Carbon UD Prepreg and Epoxy/glass fiber UD prepreg QI to improve structural performance and aerodynamic efficiency of the AAI Shadow-200 RQ-7 UAV wing will be investigated. An accurate CAD model of the wing will be generated using SolidWorks software, and comprehensive numerical analyses with ANSYS will be performed to study the aerodynamic behavior using computational fluid dynamics (CFD), to study the structural response under aerodynamic loads using fluid-structure interaction (FSI), and to determine the vibrational characteristics of the wing with and without composite materials using modal analysis. The goal is to compare the performance of the composite wing configurations against the conventional aluminum wing design, to determine the optimal composite material configuration, and to supply valuable information to industry for the design and development of advanced UAV wings.

2. Methodology

The comprehensive design and numerical analysis of the AAI Shadow-200 RQ-7 unmanned aerial vehicle (UAV) wing are presented in this section. The UAV is designed with dimensions like the market offers, but not exactly, enabling a novel design approach. The AAI Shadow-200 RQ 7 UAV wing is modeled in detail using SolidWorks, a powerful computer aided design (CAD) software. A finite element analysis (FEA) software package ANSYS is used for the numerical analysis to investigate the wing's structural performance, aerodynamic efficiency, and vibrational characteristics. The governing equations and the criteria for each type of analysis are introduced prior to the analysis. The methodology consists of design process, computational fluid dynamics (CFD) analysis, fluid-structure interaction (FSI) analysis and modal analysis. Advanced composite materials, Epoxy Carbon UD Prepreg and Epoxy/glass fibre UD Prepreg QI are integrated to improve the structural performance and the aerodynamic efficiency of the AAI Shadow-200 RQ-7 UAV wing.

A. Computational Fluid Dynamics

Computational Fluid Dynamics (CFD) is based the numerical methods and algorithms applied to solve fluid mechanics problems. CFD has become indispensable in many industries, allowing to obtain detailed information about complex fluid flow phenomena that would be difficult to obtain in practice. The availability of user-friendly commercial software packages combined with the continuing increase in computational power has fueled a rapid growth in CFD. Using CFD engineers and researchers can design, optimize and study the behavior of fluids in a wide variety of applications in aerospace and automotive engineering, biomedical and environmental sciences.

1) CAD Desing of Petroleum Pipelines

a) Continuity Equation

The Continuity Equation expresses the principle of mass conservation within a fluid flow [15]:

$$\frac{\partial \rho}{\partial t} + \nabla \cdot (\rho \vec{v}) = 0 \qquad (1)$$

ρ is fluid density (mass/volume), which quantifies how much mass there is in a unit volume of fluid; $\vec{v}$ is the flow velocity vector (distance/time) that conceptualizes area vs.

flow-rate; $\frac{\partial}{\partial t}$ is the time partial derivative, that says how the density values change with time at a point; $\nabla.$ is divergence operator that measures amount of "mass" exiting a volume at a point as a function of the velocity field.

b) Momentum Equation

$$\frac{\partial(\rho \mathbf{v})}{\partial t} + \nabla \cdot (\rho \mathbf{v} \otimes \mathbf{v}) = -\nabla p + \nabla \cdot \tau + \rho \mathbf{g} \quad (2)$$

where:

ρ is the fluid density,

$\mathbf{v}$ is the velocity vector,

p is the pressure,

τ is the viscous stress tensor, and

$\mathbf{g}$ is the gravitational acceleration vector.

c) Energy Equation

The Energy Equation, based on the first law of thermodynamics, describes the conservation of energy within the fluid:

$$\frac{\partial(\rho E)}{\partial t} + \nabla \cdot (\boldsymbol{v}(\rho E + p)) = \nabla \cdot (\tau \cdot \boldsymbol{v}) + \nabla \cdot \boldsymbol{q} \quad (3)$$

where:

E is the total energy per unit mass, including kinetic, internal, and potential energies, and

$\mathbf{q}$ represents the heat flux vector.

B. Fluid-Structure Interaction

Fluid structure interaction (FSI) is a complex phenomenon which describes how a deformable structure interacts with the surrounding or internal fluid flow. Within FSI, the structural geometry deforms due to the fluid pressure field and fluid domain is simultaneously affected by the structural geometry. In analyzing mechanical structures subjected to fluid forces, FSI is important because the system performance is determined by the structure's ability to withstand fluid forces. FSI can be classified into two main approaches: one-way and two-way FSI. In one-way FSI, structural deformations are considered small and are assumed to have a negligible effect on the fluid flow. In this approach, the fluid forces are transmitted to the structure without coupling of the structural response back to the fluid domain. When structural changes have little effect on the fluid flow, this method is applicable. On the other hand, two-way FSI includes the mutual interaction between fluid and structure. The structural deformations induced by the fluid pressure, and conversely the modifications of the fluid domain due to the structural deformations, produce a complex interaction that is therefore solved iteratively exchanging data between the fluid and structural domains until convergence is achieved. For engineering problems where the fluid structure interaction is important for the overall behavior of the system, two-way FSI is essential as the mutual effect is neglected otherwise may result in inaccurate predictions.

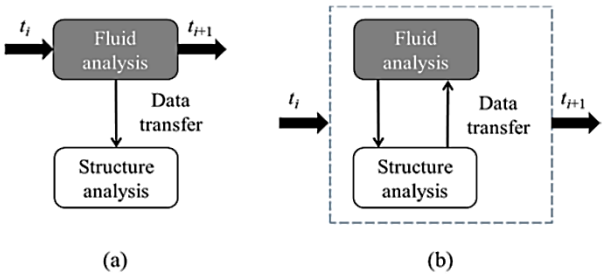

Figure 1. (a) One-way and (b) two-way interaction approaches for fluid-structure integration [16]

1. One-way FSI: Fluid forces are computed first and applied as loads on the structure, ignoring any feedback to the fluid:

$$\mathbf{F}_{\text{fluid}} = \int_{\partial \Omega_{\text{fuid}}} (p\mathbf{n} + \tau \cdot \mathbf{n}) dA \quad (4)$$

where $\mathbf{n}$ is the normal vector to the surface.

2. Two-way FSI: The interaction considers both domains, where fluid pressure influences structural deformation and deformation affects fluid flow, solved iteratively:

$$\mathbf{F}_{\text{fluid}} = \mathbf{F}_{\text{structure}}, \mathbf{v}_{\text{fluid}} = \mathbf{v}_{\text{structure}} \quad (5)$$

C. Finite Element Method

We discuss the Finite Element Method (FEM), a powerful numerical technique for solving complex engineering and mathematical physics problems. Large systems are discretized into smaller, manageable elements, and we approximate solution for each element using FEM. The broad use of this method is for structural analysis, heat transfer, fluid dynamics, and electromagnetic applications.

The FEM process consists of three main phases: The processes include preprocessing, solution, and postprocessing [17]. The domain is discretized, shape functions are assumed and element equations are developed in the preprocessing phase, followed by application of boundary conditions. Solving the system of equations is the solution phase and then analysis of the results and steps for improvement and more research is the postprocessing phase [18].

D. Composite Material

From the combination of two or more different substances comes the composite material, a key step forward in the science of materials. They do this by combining fibers or particles with matrices such as polymers, metals, or ceramics to achieve characteristics superior to those of their constituent ingredients alone. Moving from bulk components to the use of carbon nanotubes and nanofibers is a huge step in technology and shows the wide spread influence that composites have in many areas [19]. They have pronounced utility in modern engineering, especially in offering improved stiffness, elasticity, and durability with a light weight profile. Synthesis of strength, stability and lightweight properties in composite materials like carbon fibre reinforced composites (CFRC) and glass reinforced plastic (GRP) is particularly remarkable in aerospace industry where aircraft performance and efficiency are significantly improved. [20].

1) Failure Criteria

a) Maximum stress criterion

The Maximum Stress Criterion for orthotropic laminae is an extension of maximum standard stress theory applied to isotropic materials. In the case that any of the principal stress components along the material axis is larger than the corresponding strength, this criterion fails. The conditions for a composite material not to fail according to the Maximum Stress Criterion are expressed as [19] :

For longitudinal stress (σ_1) (along the fiber direction):

$$-sL(-) < \sigma_1 < sL(+) \quad (6)$$

For transverse stress (σ_2) (perpendicular to the fiber direction):

$$-sT(-) < \sigma_2 < sT(+) \quad (7)$$

For shear stress τ_{12} (in the plane of the lamina):

$$|\tau_{12}| < sLT \quad (8)$$

where $\mathrm{sL}(+)$ and $-\mathrm{sL}(-)$ are the tensile and compressive strengths in the longitudinal direction, respectively. $sT(+)$ and $-\mathrm{sT}(-)$ are the tensile and compressive strengths in the transverse direction, respectively, and sLT is the shear strength.

b) Maximum strain criterion

The Maximum Strain Criterion, introduced in 1967, is used to forecast the failure of orthotropic laminae so that it is considered as an extension of the maximum normal strain theory for isotropic materials. This factor states that failure happens when any principal material axis strain component exceeds the corresponding ultimate strain. To avoid failure under this criterion, the material must satisfy the following inequalities [19]:

The longitudinal strain ε 1 must remain within the bounds of the ultimate compressive strain −eL(−) and the ultimate tensile strain eL(+). The transverse strain ε 2 must stay within the limits set by the ultimate compressive strain −eT(−) and the ultimate tensile strain eT(+). The absolute value of the shear strain γ 12 must not exceed the ultimate shear strain let [19].

$$-eL(-) < \varepsilon_1 < eL(+) \quad (9)$$

$$-eT(-) < \varepsilon_2 < eT(+) \quad (10)$$

$$|\gamma_{12}| < eLT \quad (11)$$

c) Tsai-Wu failure criterion

The Tsai-Wu failure criterion provides a universal way of failure prediction of anisotropic materials, such as composites, by considering the intricate interrelations of various stress components. This criterion is particularly convenient for engineering of composite materials because materials tend to

have strength in different directions because of their anisotropic character [19].

$$F_i\sigma_i + F_{ij}\sigma_i\sigma_j = 1 \quad (12)$$

In this equation, i,j= 1,2,…6 correspond to the stress components in a contracted notation, and F_i and F_{ij} are material-specific constants determined through experimentation. This criterion considers both the individual stress components and their interactions. To predict failure accurately, the criterion stipulates that the equation's left side must not exceed 1, with failure predicted when this value reaches or surpasses 1.

d) Tsai-Hill failure criterion

The Tsai-Hill criterion reduces the Tsai-Wu criterion under certain assumptions regarding equal tensile and compressive strengths for predicting failure in composite materials. This criterion is based on the von Mises yield criterion and is modified to consider the anisotropy in composite materials [19].For cases of plane stress, where $\sigma_3, \sigma_{33}, \sigma_{34}, \sigma_{35} = 0$ the Tsai-Wu criterion simplifies to [19]:

$$F_{11}\sigma_1^2 + F_{22}\sigma_2^2 + F_{66}\tau_{12}^2 + F_1\sigma_1 + F_2\sigma_2 + 2F_{12}\sigma_1\sigma_2 = 1 \quad (13)$$

Here, F_{11}, F_{22}, F_{66}, F_1, F_2, and F_{12} are the material constants for the composite, σ_1 and σ_2 are the normal stresses, and τ_{12} is the shear stress in the plane of the lamina.

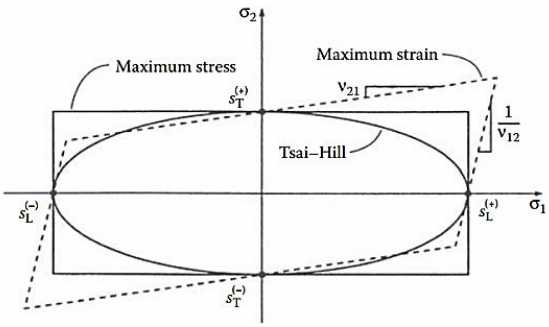

Figure 2. Shows the failure surfaces for the Maximum Stress, Maximum Strain, and Tsai-Hill criteria in σ_1 , σ_2 stress space, demonstrating how each criterion predicts material failure under different stress conditions [19]

e) Safety factor

The safety factor, a main engineering principle, ensures that a component remains operational under specified conditions by maintaining a margin of safety against load increases or strength decreases. This built-in margin accounts for uncertainties in load, strength, material properties, and unforeseen stresses, safeguarding against failure. It is calculated by comparing the component's strength to its expected load [21].

$$n = \frac{S}{\sigma} \quad (14)$$

If the n > 1 The composite is safe and If the n < 1 The composite fails.

f) Inverse reverse factor

The Inverse Reverse Factor (IRF) is proposed as a critical parameter to evaluate the failure susceptibility of the composite materials. IRF is employed to forecast composite failure, that is the load value/ IRF. There are two cases for it [22]:

IRF > 1: The composite fails and IRF < 1: The composite is safe.

E. Natural Frequency

Natural frequency analysis is a technique that is utilized to identify the frequencies at which drives vibrate or structural components self-oscillate due to an intrinsic vibration under conditions of a disturbance [23]. Numerical analysis is crucial for identifying resonant frequencies in UAV fixed wings, which, if matched with operational vibrations, can compromise structural integrity and safety. Avoiding these frequencies is key to preventing flutter, an uncontrollable oscillation that can lead to failure, ensuring UAVs remain stable and safe during operation.

1) Natural Frequency Formulas

a) General Formula for Natural Frequency [23].

$$f = \frac{1}{2\pi}\sqrt{\frac{EI}{\mu}} \quad (15)$$

The natural frequency (f) of a wing of a UAV can be obtained through this equation, where E denotes the Young's modulus of the material (stiffness), I stand for the second moment of inertia of the cross-section of the wing (bending resistance), and μ is the mass per unit length of the wing. This equation emphasizes

that the vibrational properties of a wing are closely connected with its materials properties and mass distribution [23].

b) Mass per Unit Length (μ)

$$\mu = \rho A + \mu_{\text{additional}} \quad (16)$$

This equation determines the wing mass per unit length of a UAV. ρ wing the density of the wing material, Area A is, and μ additional considers any excess weight from the components or the payloads which are embedded within the wing. This equation makes sure that the inherent weight of the wing and the added weight from equipment or payload are considered in the analysis [23].

F. AAI Shadow -200 RQ-7 UAV Design

The software used in this research for the UAV model design is SOLIDWORKS. The design of the UAV will be like the actual form and sizes available on the market, with slight changes. These changes will provide an opportunity for the aspect of new dimensions, including the analysis of composite materials, to be trialled since this is the main subject of this research.

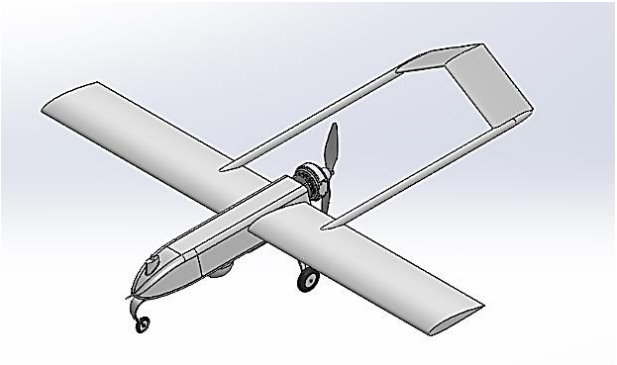

Figure 3. AAI Shadow -200 RQ-7 UAV Model

Table 1: Dimensions of RQ-7 UAV

Parameter	Value
Length	3.98 m
Height	2 m
Wingspan	4.43 m

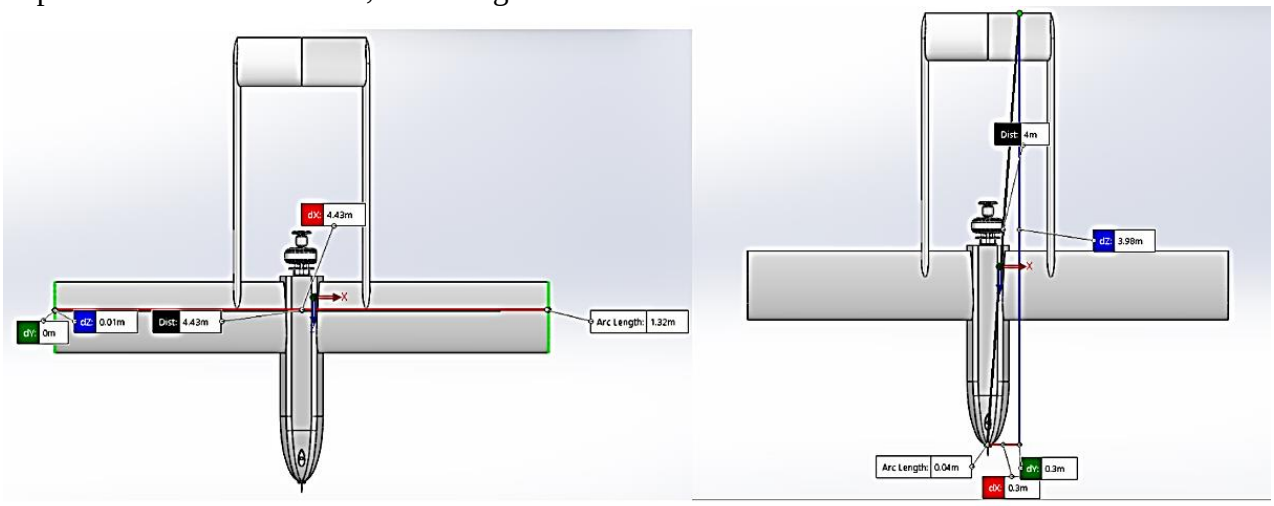

(a) (b)

Figure 4. (a) Dimensions of wingspan, (b) Dimensions of total length

However, the study will be conducted on the UAV's wing because it is the most appropriate part to place composite materials on. Therefore, the wing was separated from the plane, as the picture below shows.

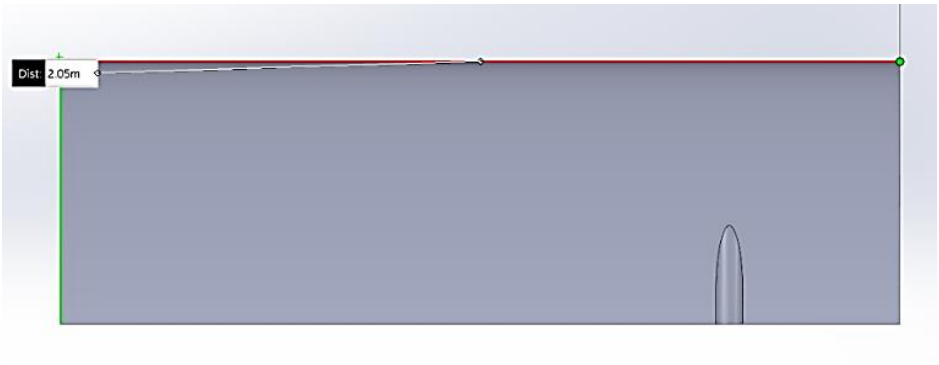

Figure 5. AAI Shadow -200 RQ-7 wing length

ANSYS software studies the CFD on a UAV, but before that, the UAV's wing is placed in the fluid domain designed by SOLIDWORKS to form a tunnel for the air to be studied in the next section, which is what the figures below show.

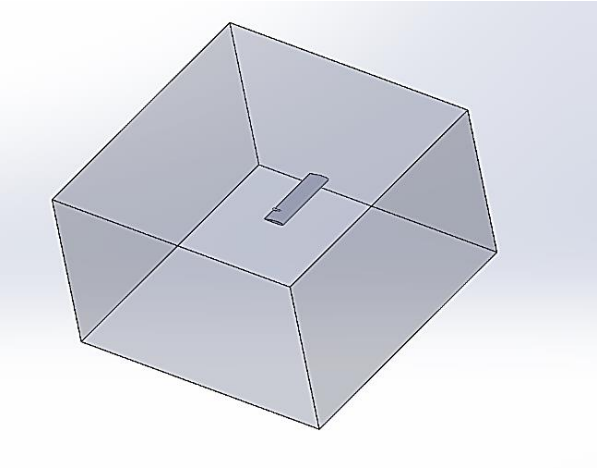

Figure 6. AAI Shadow -200 RQ-7 wing length (all domain)

Table 2: Properties of the fluid domain

Parameter	Value
Total Domain Length	12 m
Total Domain Width	12 m
Total Domain Hight	5 m

G. AAI Shadow -200 RQ-7 UAV Numerical Analysis

1) CFD analysis

The first step is to create a mesh for the fluid domain around the UAV wing to get precise results in CFD analysis. Mesh settings and quality metrics are important for achieving an accurate and reproducible outcome. The figures and table that follow indicate the mesh generation process and its settings.

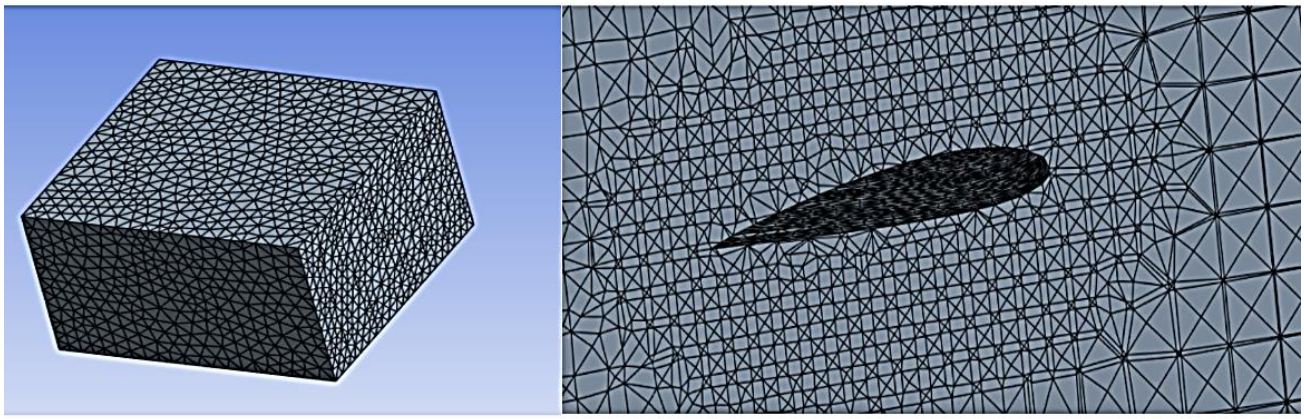

(a) (b)

Figure 7. (a) Mesh results on a whole fluid domain, (b) Mesh results on a whole fluid domain

The mesh settings used are in the table below.

Table 3: Mesh Settings for Fluid Domain

Mesh Method	**Tetrahedrons**
Algorithm	Patch independent
Max Element Size	400 mm
Min Element Size	70 mm
Face sizing	50 mm

To check the reliability of the simulation, a grid independence test was performed where the mesh size was changed. This research used three mesh densities: coarse, medium, and fine, in which drag coefficient, lift coefficient, and the maximum deformation were measured and analyzed. The results have indicated that for a mesh density higher than the medium the values of these parameters became grid independent. Therefore, this medium mesh was decided for further analysis since it provides balance between the details and time consumption.

The boundary conditions for the CFD analysis were appropriately defined to represent the fluid domain and flow conditions accurately. The inlet of the fluid domain was specified as a velocity-inlet, the outlet as a pressure-outlet, and the wing body and remaining surfaces as wall boundaries. These boundary conditions ensure that the flow physics is correctly captured in the computational domain, allowing for reliable and physically meaningful results from the CFD simulations.

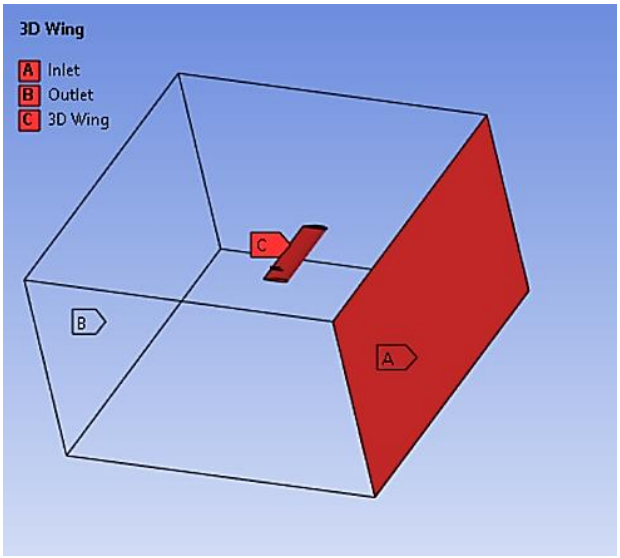

Figure 8. Boundary conditions of fluid domain for RQ-7

After completing the mesh, the analysis settings were defined in Setup and presented in the table below.

Table 4: ANSYS fluent analysis setup settings

Iterations	1000
Scheme	coupled
Gradient	Least Squares Cells Based
Pressure	Second Order
Viscous Mode	k-epsilon (eqn) Realizable

As discussed in the introduction of this section, the study was conducted at the UAV's

maximum speed to ensure a more accurate structural analysis. According to previous research, the RQ-7 UAV's maximum speed is 218 km/h [24].

2) FSI Analysis

This analysis will require a 3D solid aluminum wing. As previously mentioned, the first step will be generating a wing mesh.

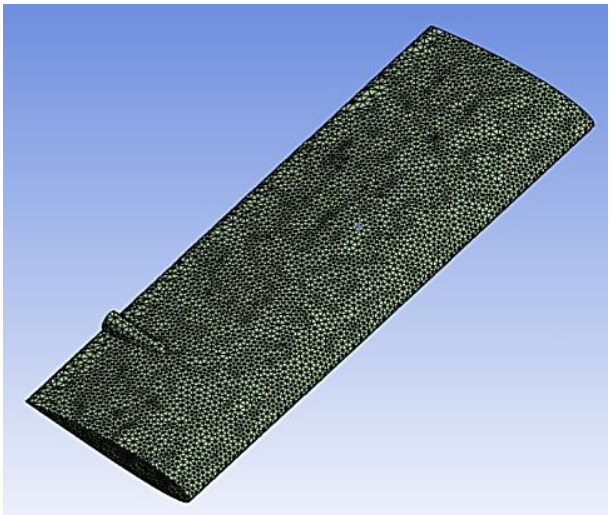

Figure 9. Mesh results on 3D wing of RQ-7 UAV

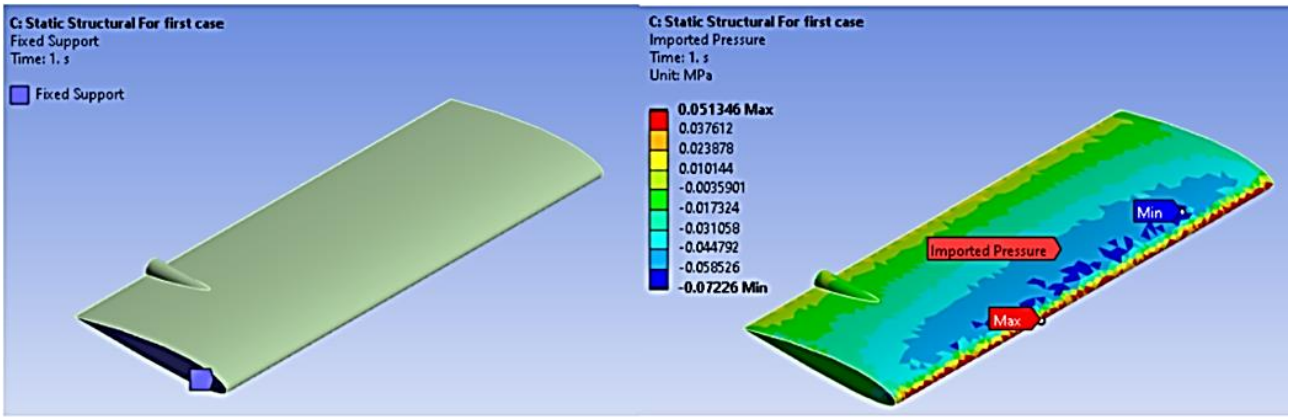

(a) (b)

Figure 10. (a) shows the fixed support and (b) The Imported pressure load on the RQ-7 UAV

3) ACP Composite Materials Analysis

The ACP (ANSYS Composite PrepPost) module will be used for composite analysis in UAV wing case studies, enabling precise specification of material types, thicknesses, and layups. This study focuses on Epoxy Carbon UD (230 GPa) Prepreg and Epoxy/glass fiber UD prepreg, QI composites, detailed in the subsequent tables.

Table 5: Composite, Epoxy Carbon UD (230 GPa) Prepreg [25]

Density (kg/m³)	Young's Modulus (GPa)	Poisson's Ratio	Shear Strength (MPa)	Shear Modulus (GPa)	Tensile Strength (MPa)
1490	121	0.4	60	4.7	2231

Table 6: Composite, Epoxy/glass fiber, UD prepreg, QI [26]

Density (kg/m³)	Young's Modulus (GPa)	Poisson's Ratio	Shear Strength (MPa)	Shear Modulus (GPa)	Tensile Strength (MPa)
1840	21	0.31	33	9.23	504

Ten layers of composite material, each 0.5 mm thick, will be added to each composite material case, resulting in a total thickness of 5 mm on the aircraft wing.

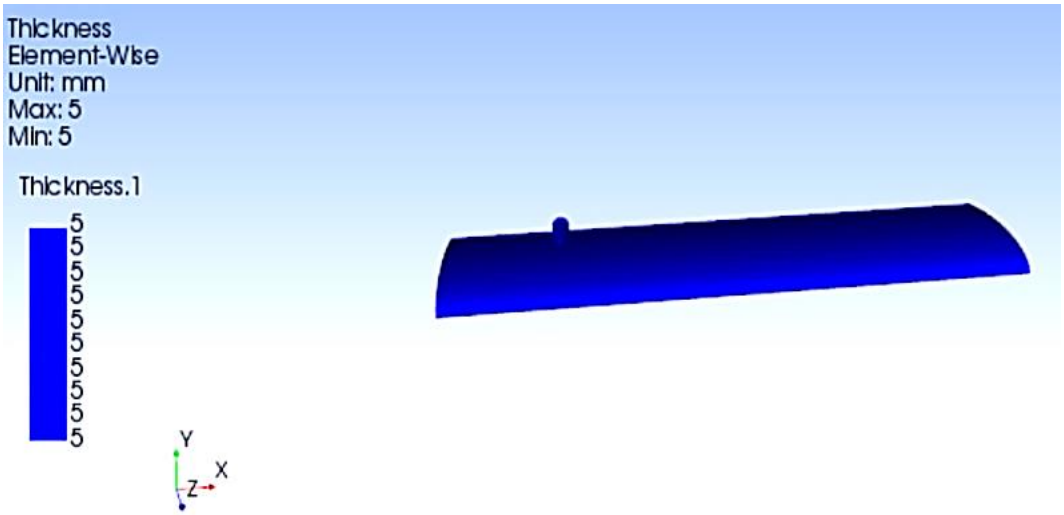

Figure 11. RQ-7 Wing after composite material added

After placing the composite material, the wing was re-linked in the Static Structure window to transfer the properties of the composite material to the FSI analysis and obtain the results.

4) Modal Analysis

The analysis will utilize ANSYS's Modal Analysis module to examine the UAV wing's natural frequencies, integrating findings with the FSI Static Structural module for comprehensive frequency determination.

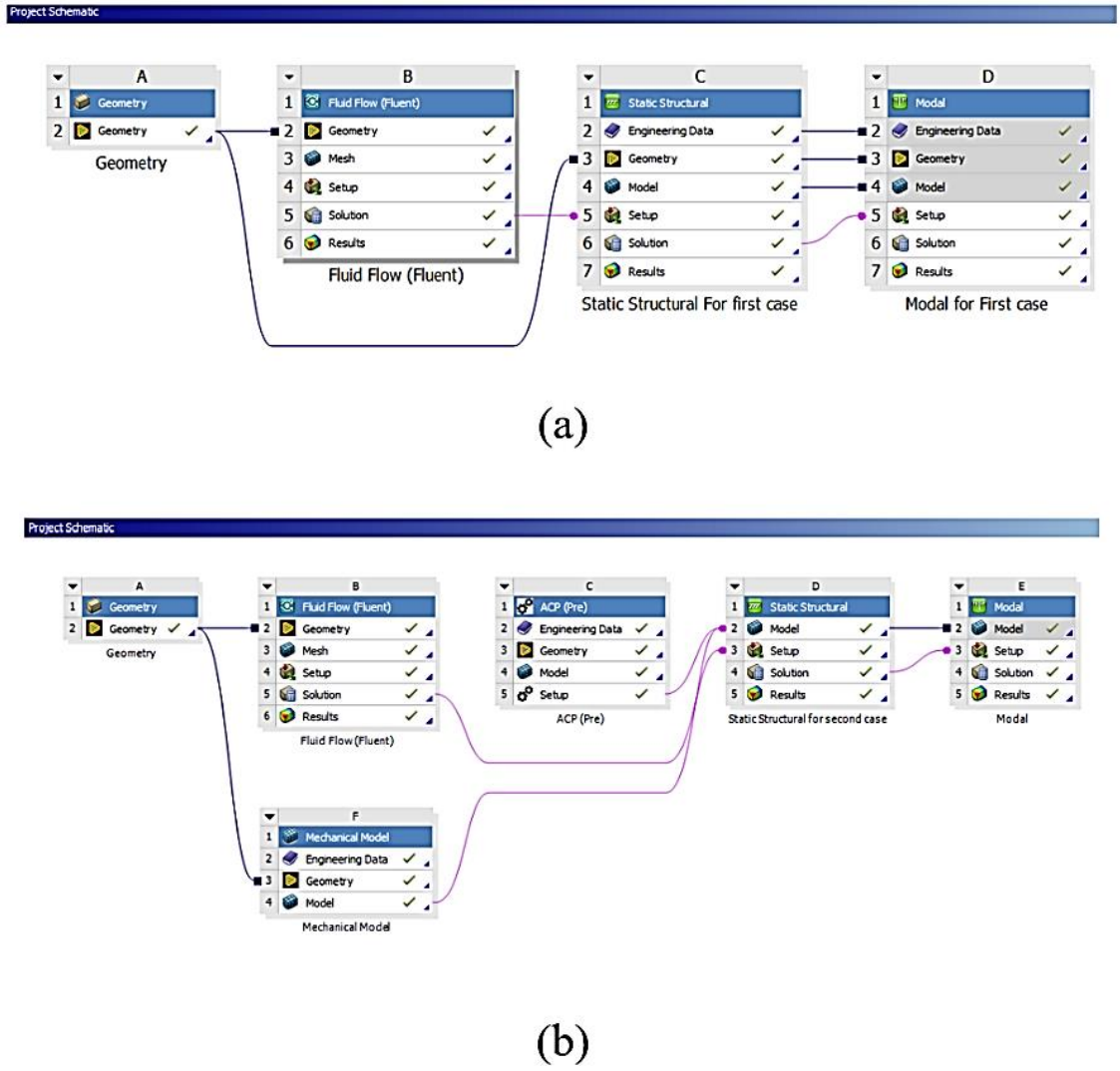

Figure 12. (a) Project schematic for the first case study, (b) Project schematic for the second and third case study

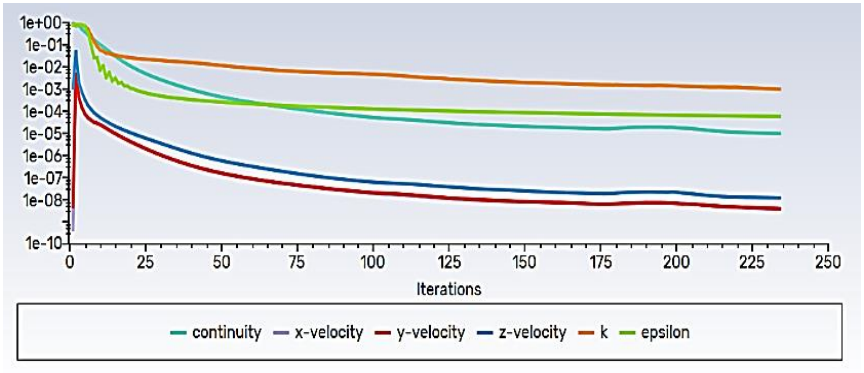

Figure 13. Convergence of solution of CFD analysis

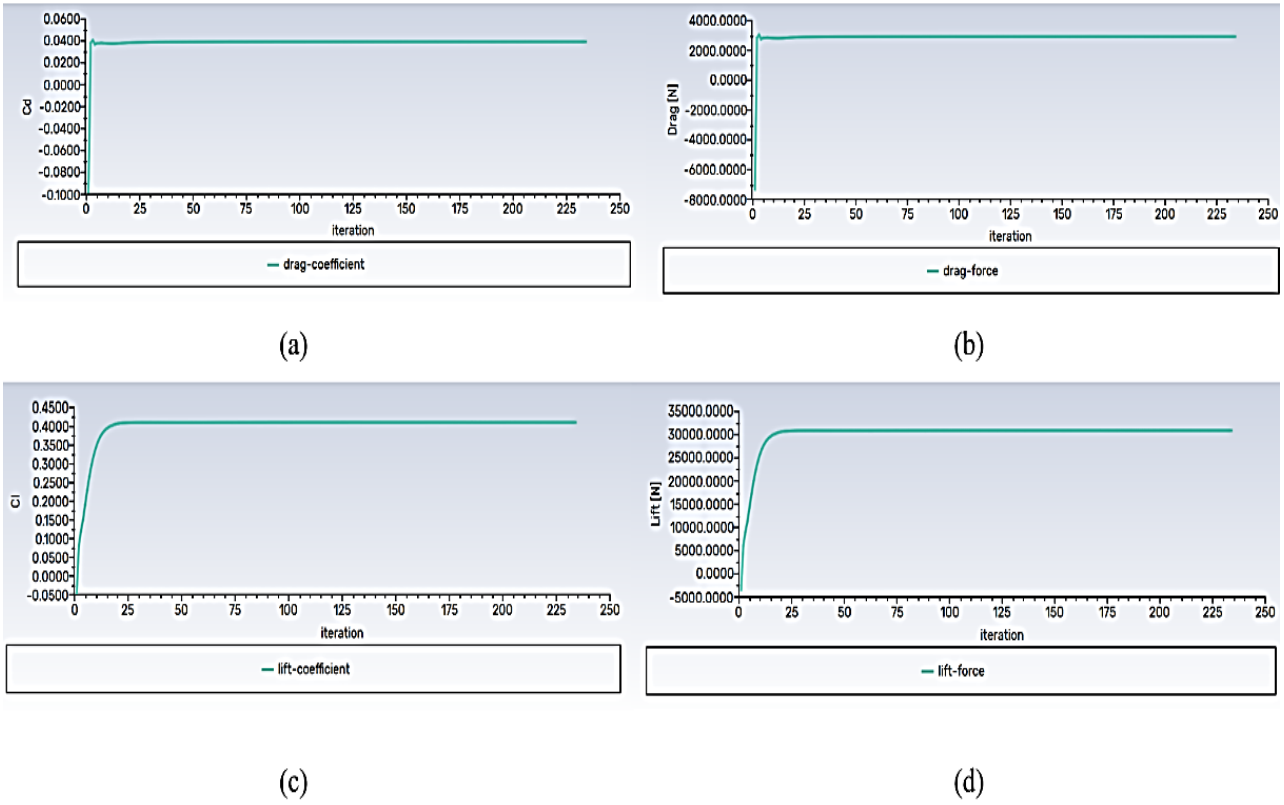

Figure 14. Values of (a) drag coefficient, (b) drag force, (c) lift coefficient, and (d) lift force against solution iterations

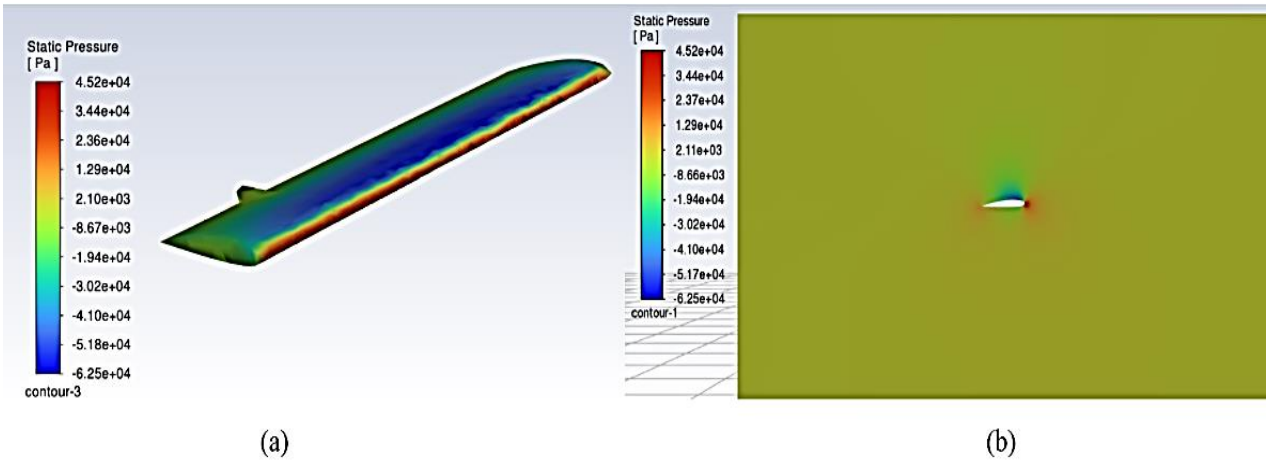

Figure 15. (a) Shows the pressure contours on the 3D wing, (b) Shows the pressure contours on the 2D section of the wing

Table 7: Results of CFD Analysis

Parameter	**Value**
Drag coefficient	0.04
Drag force	2944 (N)

Lift coefficient	0.41
Lift force	30905.83 (N)
Iterations for convergence	241

B. First Case Study

1) FSI Analysis Results

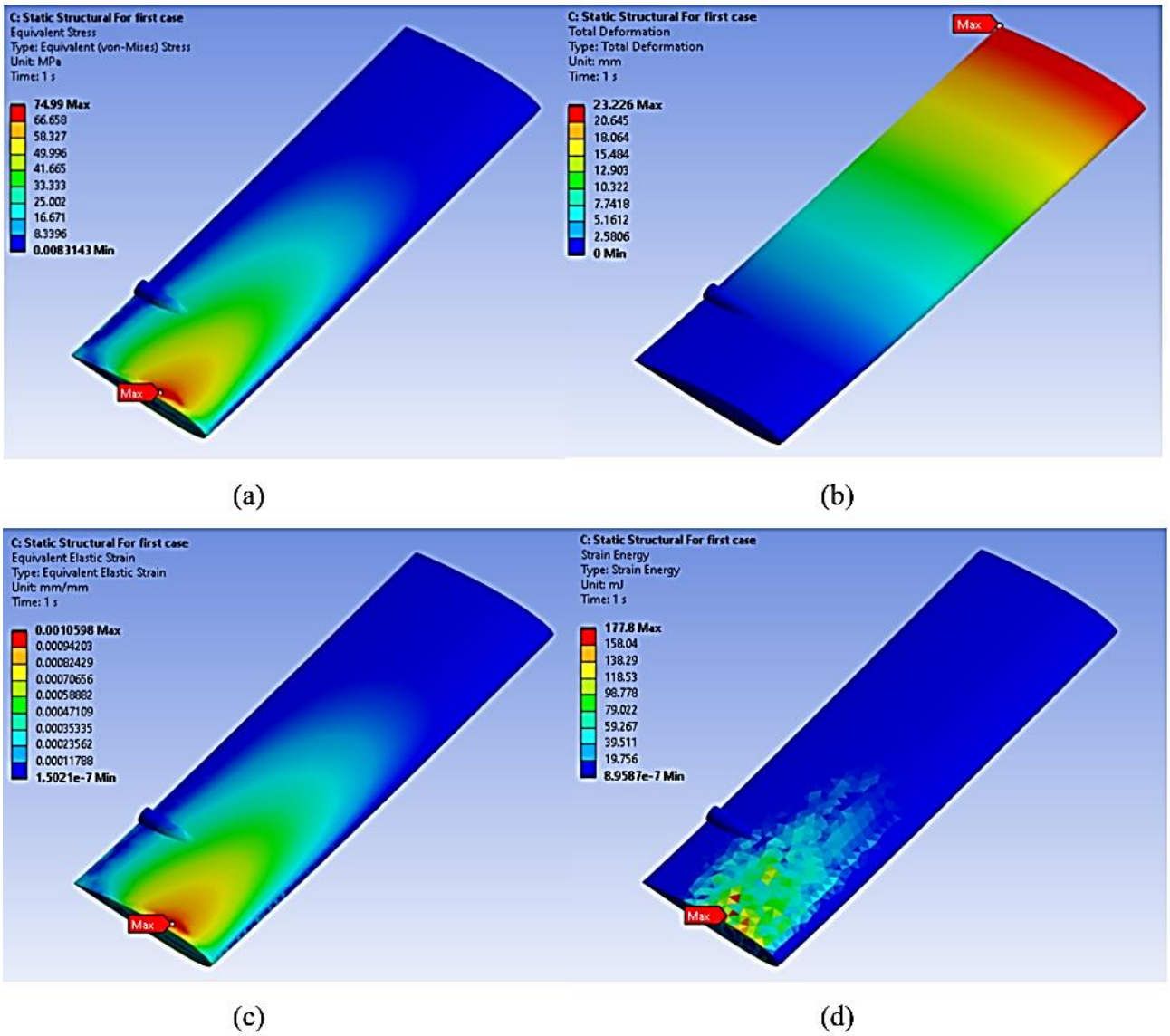

Figure 16. (a) Maximum Von-mises stress, (b) Total Deformation, (c) Equivalent Elastic Strain, and (d) Strain Energy of RQ-7 Wing when the material is aluminum

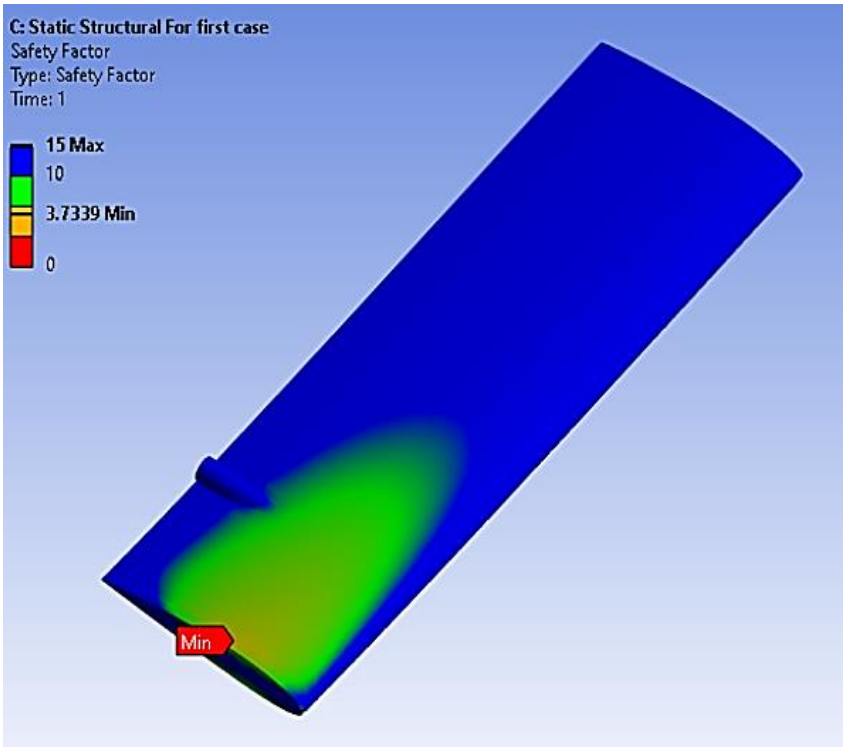

Figure 17. Safety Factor of RQ-7 Wing when the material is aluminum

2) Modal Analysis Results

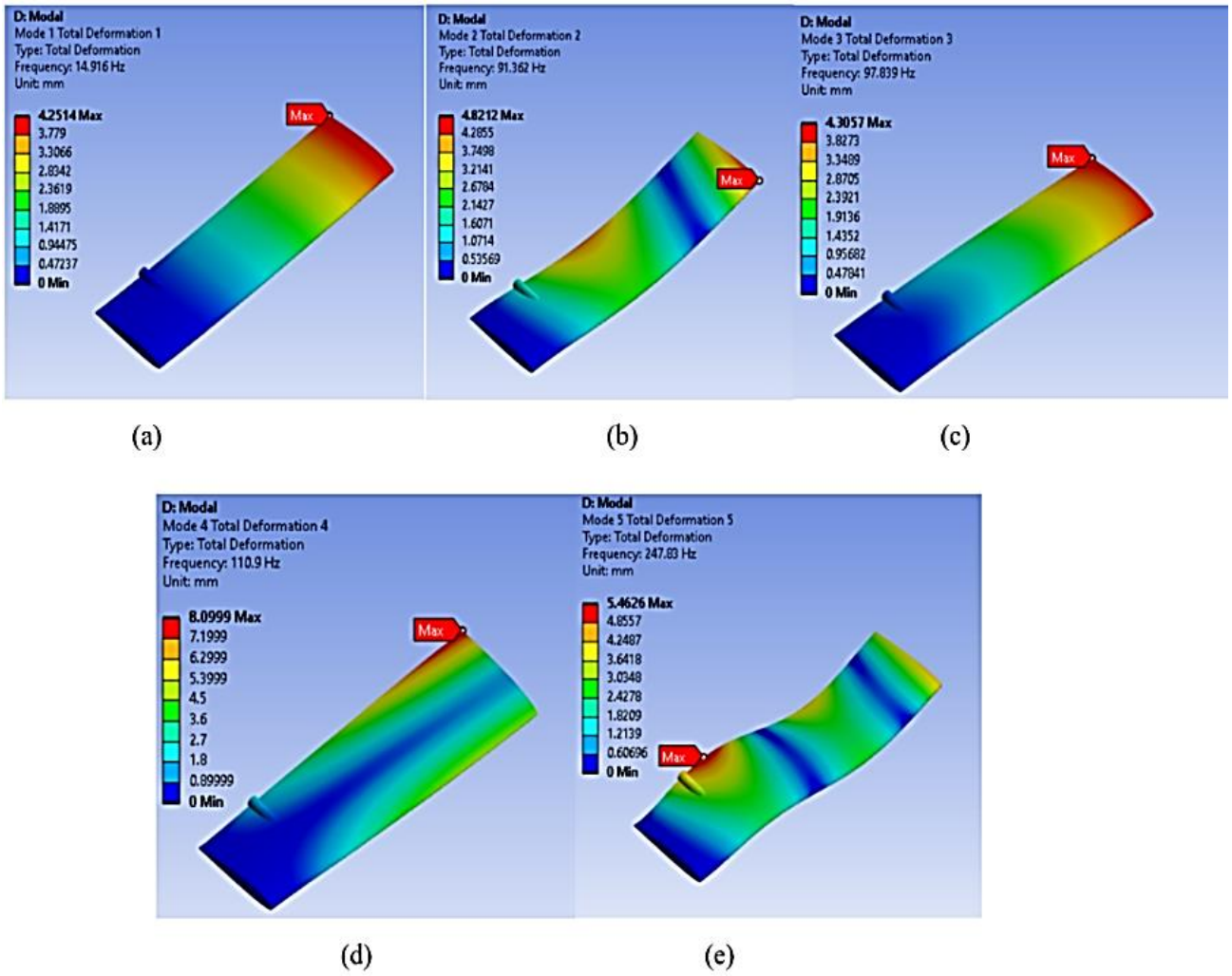

Figure 18. Modal analysis results of RQ-7 wing when the material is aluminum: (a) Mode 1, (b) Mode 2, (c) Mode 3, (d) Mode 4, (e) Mode 5

Table 8: Natural frequencies of the first case study

Mode	Frequency [Hz]	Total Deformation (mm)
1	14.916	4.25
2	91.362	4.82
3	97.839	4.30
4	110.9	8.09
5	247.83	5.46

C. Second Case Study

1) FSI Analysis Results

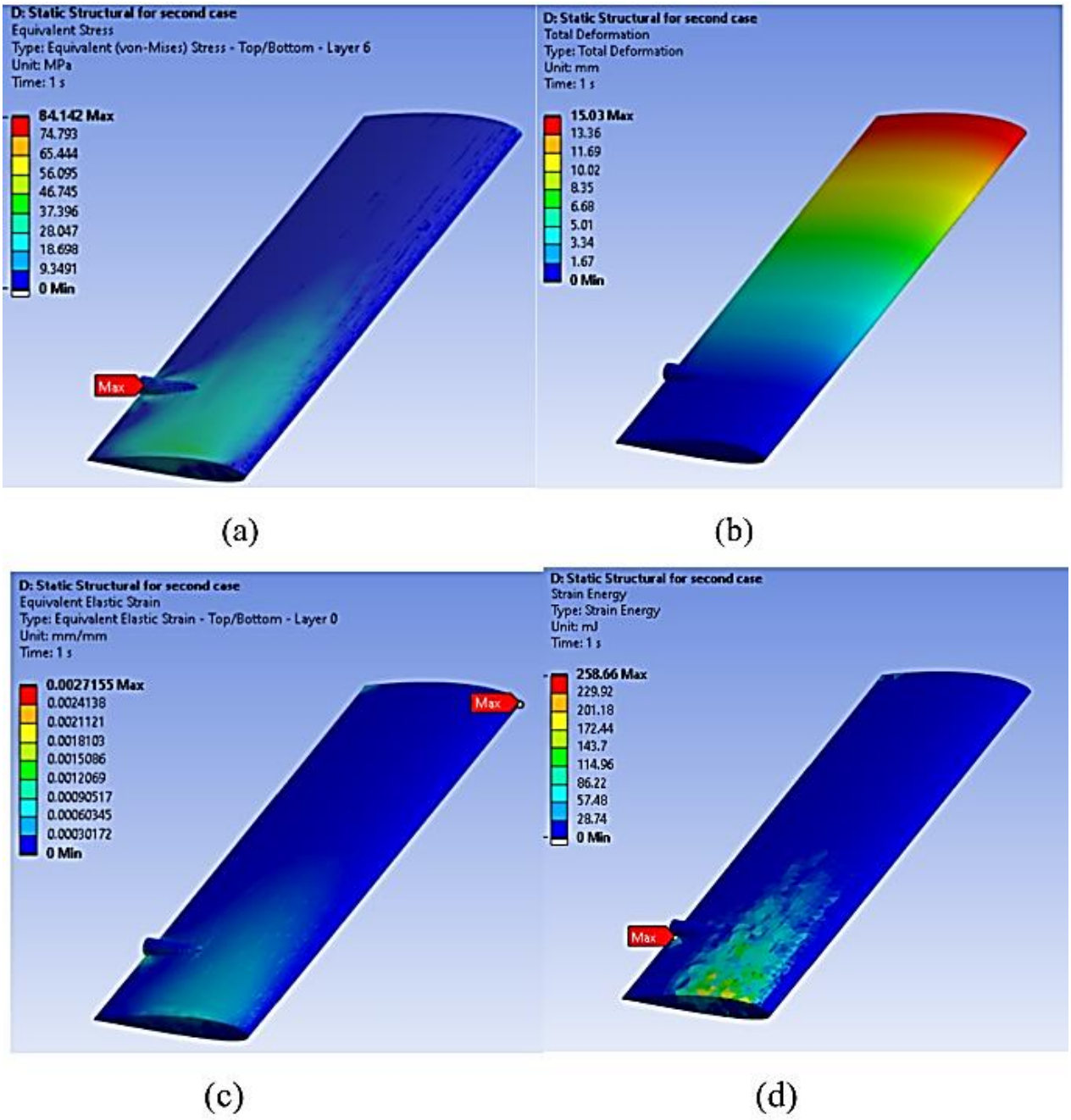

Figure 19. (a) Maximum Von-mises stress, (b) Total Deformation, (c) Equivalent Elastic Strain, and (d) Strain Energy of RQ-7 Wing when the material is Composite, Epoxy Carbon UD (230 GPa) Prepreg

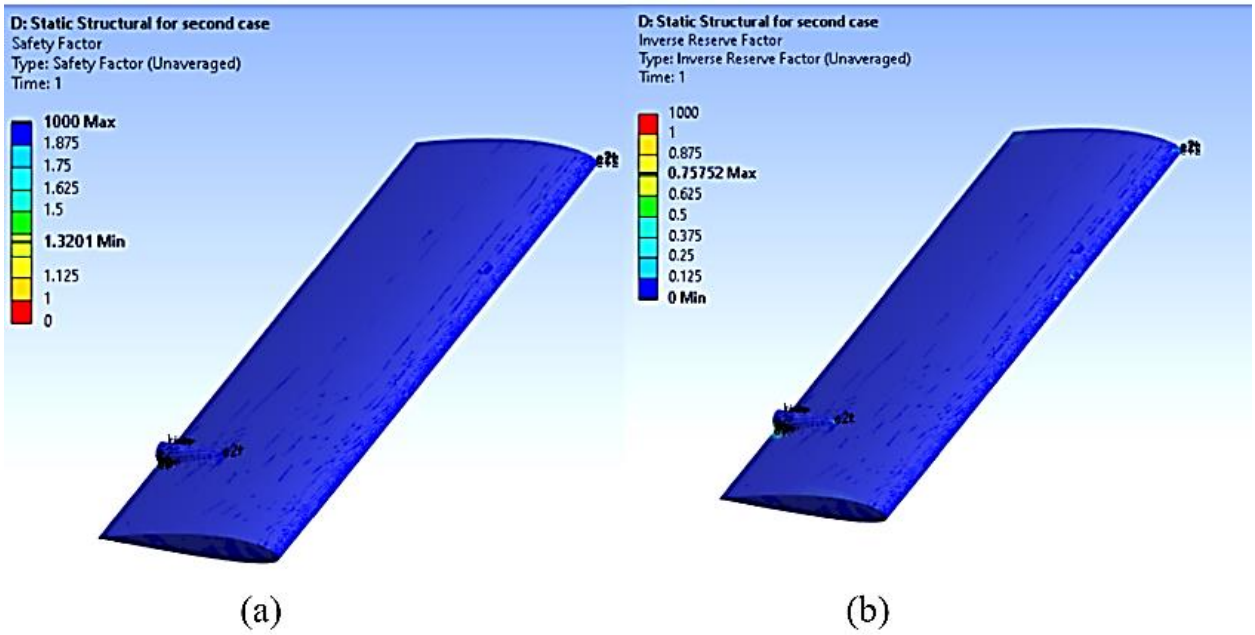

Figure 20. (a) Safety Factor, and (b) Inverse reserve factor of RQ-7 Wing when the material is Composite, Epoxy Carbon UD (230 GPa) Prepreg

Table 9: Safety factors values for different criteria for the second case

Criteria	Maximum Stress	Maximum Strain	Tsai-Wu	Tsai-Hill
Safety Factor (SF)	1.647	**1.32**	1.463	1.537

Table 10: Inverse Reserve Factor values for different criterias for second case

Criteria	Maximum Stress	Maximum Strain	Tsai-Wu	Tsai-Hill
Inverse Reserve Factor (IRF)	0.637	**0.757**	0.682	0.644

2) Modal Analysis

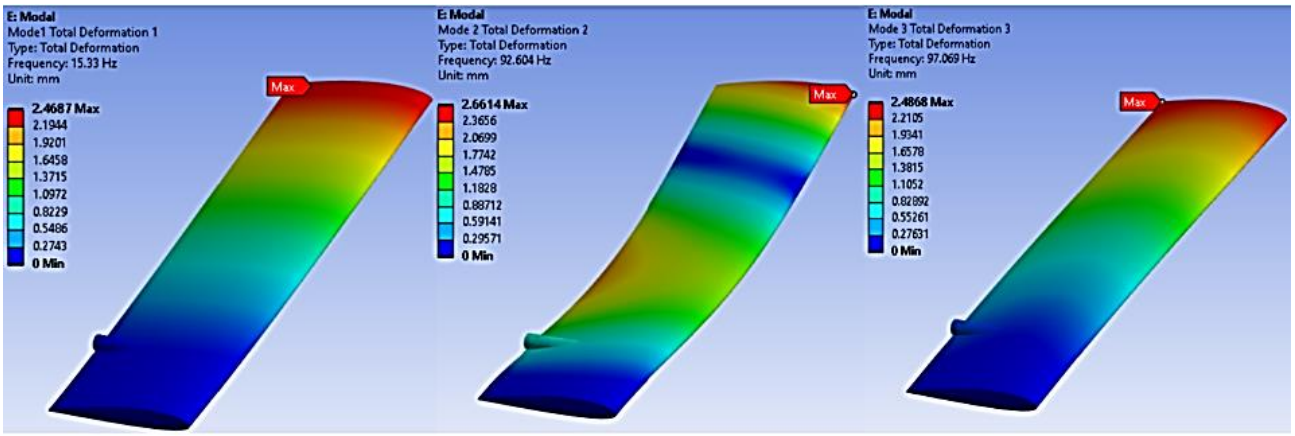

(a) (b) (c)

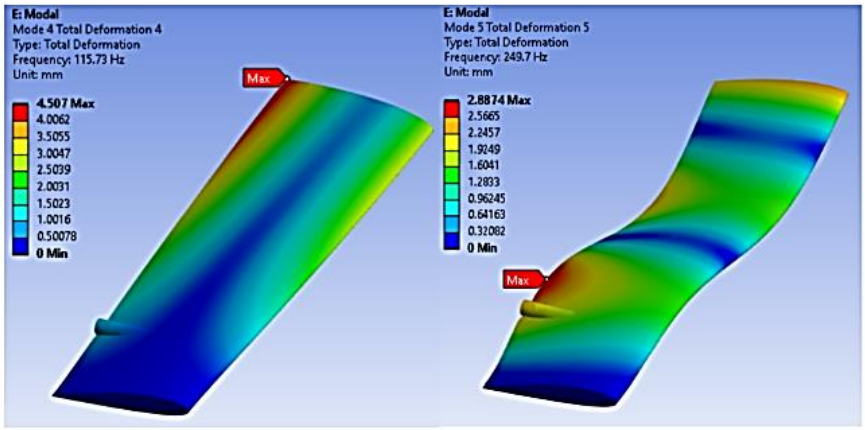

(d) (e)

Figure 21. Modal analysis results of RQ-7 wing when the material is Composite, Epoxy Carbon UD (230 GPa) Prepreg.: (a) Mode 1, (b) Mode 2, (c) Mode 3, (d) Mode 4, (e) Mode 5

Table 11: Natural frequencies of the second case study

Mode	Frequency [Hz]	Total Deformation (mm)
1	15.33	2.46
2	92.604	2.66
3	97.069	2.48
4	115.73	4.50

D. Third Case Study

1) FSI A3nalysis Results

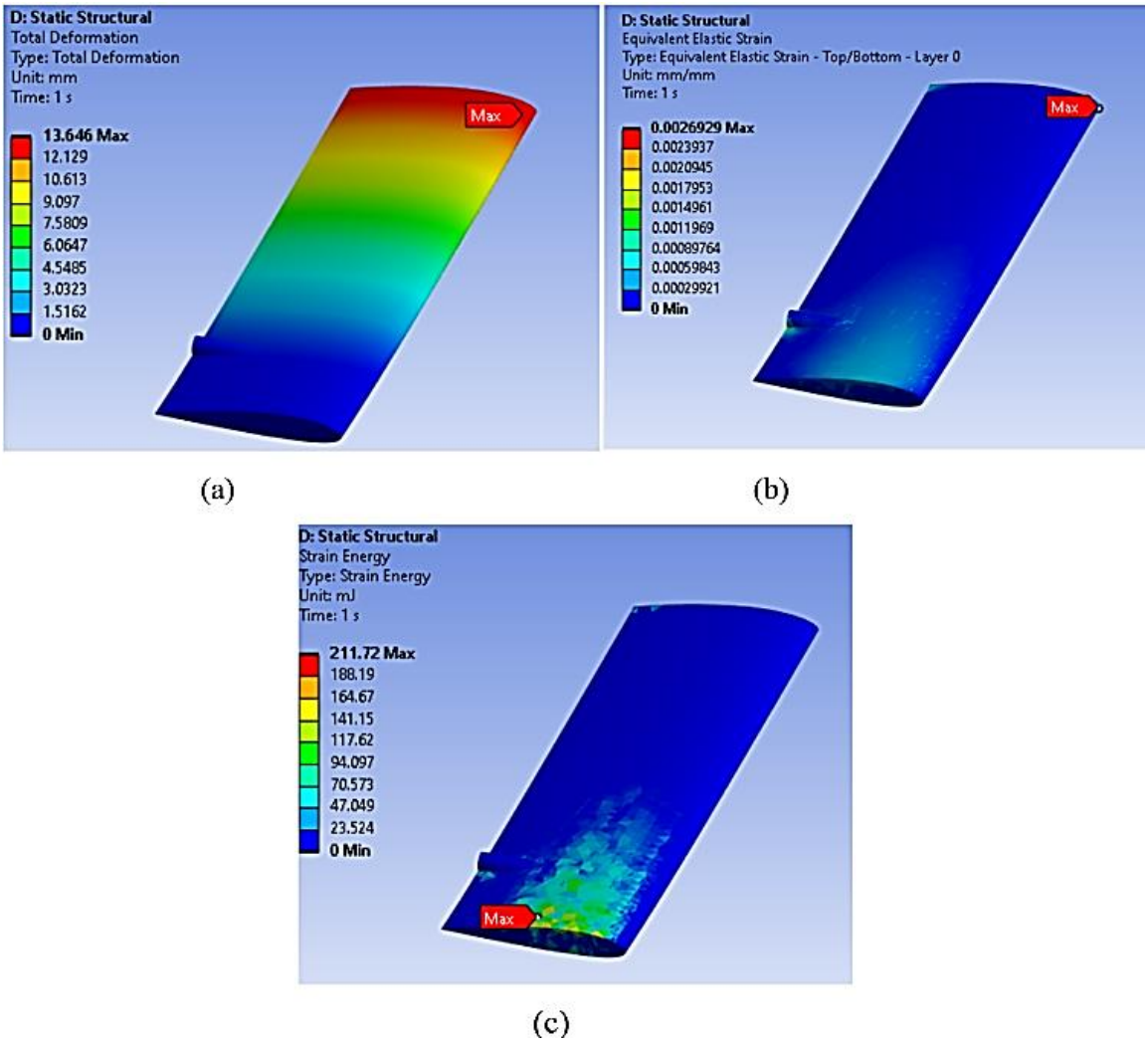

Figure 22. (a) Maximum Von-mises stress, (b) Total Deformation, and (c) Equivalent Elastic Strain of RQ-7 Wing when the material is Composite, Epoxy/glass fibre

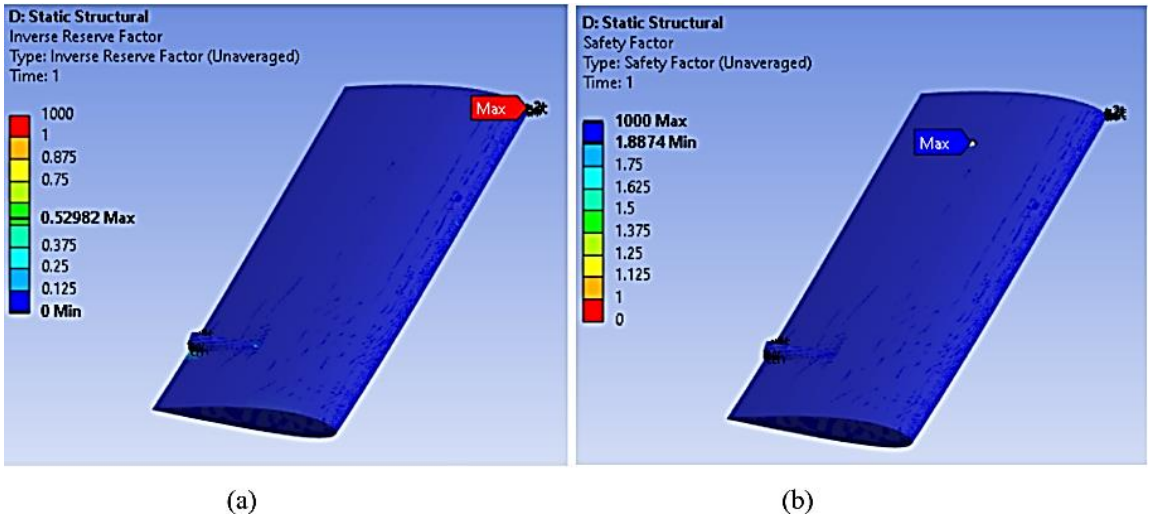

Figure 23. (a) Safety Factor, and (b) Inverse reserve factor of RQ-7 Wing when the material is Composite, Epoxy/glass fiber, UD prepreg, QI

Table 12: Total Deformation on RQ-7 Wing when the material is Composite, Epoxy/glass fiber, UD prepreg, QI

Parameter	Value
Maximum Von-mises stress	84.142 (MPa)
Total Deformation	13.646 (MPa)
Elastic strain	0.00269
Strain Energy	211.72 (mJ)
Factor of safety	1.88
Inverse Reserve Factor	0.529

Table 13: Safety factors values for different criteria's for third case

Criteria	Maximum Stress	Maximum Strain	Tsai-Wu	Tsai-Hill
Safety Factor (SF)	2.033	**1.887**	1.961	2.011

Table 14: Inverse Reserve Factor values for different criterias for third case

Criteria	Maximum Stress	Maximum Strain	Tsai-Wu	Tsai-Hill
Inverse Reserve Factor (IRF)	0.491	**0.529**	0.509	0.497

2) Modal Analysis Results

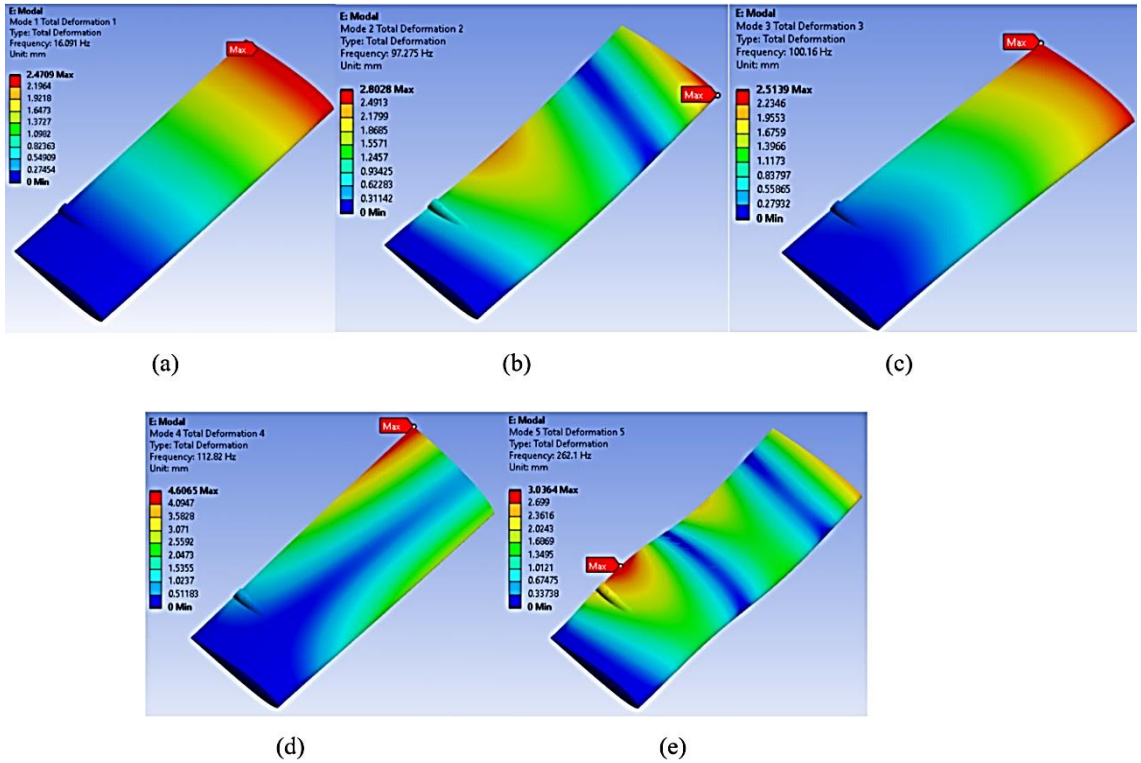

Figure 24. Modal analysis results of RQ-7 wing when the material is Composite, Epoxy/glass fiber, UD prepreg, QI. (a) Mode 1, (b) Mode 2, (c) Mode 3, (d) Mode 4, (e) Mode 5

Table 15: Natural frequencies of the third case study

Mode	Frequency [Hz]	Total Deformation (mm)
1	١٦.٠٩١	2.٤٧
2	9٧.٢٧٥	2.٨٠
3	١٠٠.١٦	2.٥١
4	١١٢.٨٢	4.٦0
5	٢٦٢.١	٣.٠٣

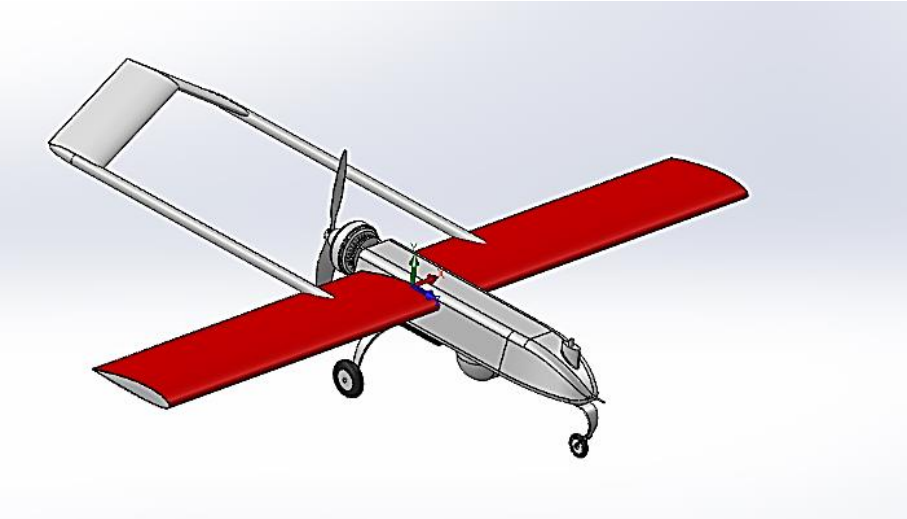

Figure 25. AAI Shadow -200 RQ-7 UAV Model after adding composite material

The second and third case studies, employing different composite materials, demonstrate good structural performance and meet safety requirements. The third case, using Epoxy/glass fibre, UD prepreg, QI, proves superior to the second case, which uses Epoxy Carbon UD (230 GPa) Prepreg. The third case exhibits a higher safety factor (1.88), a lower inverse reserve factor (0.529), and lower total deformation (13.646 MPa) compared to the second case (15.03 MPa), indicating better structural response and load-carrying capacity. Consequently, the Epoxy/glass fibre, UD prepreg, QI composite used in the third case is the most advantageous option for the aircraft wing structure, offering superior performance, improved safety margins, and better overall economy. The natural frequencies of second and third cases are close to each other and two composite materials have similar effects on vibrational characteristics of wing, as shown by the modal analysis.

4. Conclusions

In this context, the current work proves that the Epoxy Carbon UD Prepreg and Epoxy/glass fiber UD prepreg QI improve the structural stiffness and aerodynamic characteristics of UAV wings based on a detailed numerical analysis. The analysis of results shows that QI composite material of epoxy/glass fiber UD prepreg has higher safety factor, lesser deformation and more load carrying capacity than conventional aluminum material. Furthermore, from modal analysis it is found that both composites offer comparable vibrational damping which is essential for UAV application in different flight situations. These findings suggest that advanced composites can enhance the design of UAV wing and indicate its application for the further development of the aerospace industry. Further composite

configurations should be explored in future work and the durability of the environment should be assessed for long-term efficiency.

Conflict of interest

The authors declare that there is no conflict of interest regarding the publication of this paper.

Ethical approval

The authors declare no ethical approval is required.

References

[1] P. G. Fahlstrom and T. J. Gleason, Introduction to UAV Systems, 4th ed. West Sussex: Wiley & Sons, Inc., 2012.

[2] M. Palik and M. Nagy, "Brief history of UAV development," Repüléstudományi Közlemények, vol. 31, no. 1, pp. 155–166, 2019, doi: 10.32560/rk.2019.1.13.

[3] H. Nawaz, H. M. Ali, and S. Massan, "APPLICATIONS OF UNMANNED AERIAL VEHICLES : A REVIEW," in Tecnología. Glosas de innovación aplicadas a la pyme. Edición Especial, Noviembre, 2019, pp. 85–105. doi: 10.17993/3ctecno.2019.specialissue3.85-105.

[4] H. Sharma, C. S. Suraj, R. Antony, G. Ramesh, S. Ahmed, and P. Narayan, "Design of a High Altitude Fixed Wing Mini UAV-Aerodynamic Challenges," 2013.

[5] J. Yu, "Design and Optimization of Wing Structure for a Fixed-Wing Unmanned Aerial Vehicle (UAV)," Modern Mechanical Engineering, vol. 08, no. 04, pp. 249–263, 2018, doi: 10.4236/mme.2018.84017.

[6] S. Syam Narayanan, R. A. Ahmed, M. E. Varshini, V. B. Rao, and S. Kyathiswar, "One-way fluid-material interaction study on a plunging UAV wing," in Materials Today: Proceedings, Elsevier Ltd, 2021, pp. 316–320. doi: 10.1016/j.matpr.2021.07.408.

[7] A. N et al., "Design and analysis of a tail sitter (VTOL) UAV composite wing," Mater Today Proc, vol. 56, pp. 1604–1613, 2022, doi: 10.1016/j.matpr.2022.03.231.

[8] E. I. Basri, A. A. Basri, S. Balakrishnan, M. T. H. H. Sultan, and K. A. Ahmad, "Performance analysis of composite laminates wing skin with the aid of fluid structure interaction of aerodynamic loading-structural analysis," Mechanics Based Design of Structures and Machines, vol. 52, no. 2, pp. 922–942, 2022, doi: 10.1080/15397734.2022.2126983.

[9] M. El Adawy et al., "Design and fabrication of a fixed-wing Unmanned Aerial Vehicle (UAV)," Ain Shams Engineering Journal, vol. 14, no. 9, pp. 1–17, Sep. 2023, doi: 10.1016/j.asej.2022.102094.

[10] D. Ishihara and M. Onishi, "Computational fluid–structure interaction framework for passive feathering and cambering in flapping insect wings," Int J Numer Methods Fluids, vol. 96, no. 5, pp. 435–481, Apr. 2023, doi: 10.1002/fld.5251.

[11] Y. Wang, P. Lei, B. Lv, Y. Li, and H. Guo, "Study on Fluid–Structure Interaction of a Camber Morphing Wing," Vibration, vol. 6, no. 4, pp. 1060–1074, Dec. 2023, doi: 10.3390/vibration6040062.

[12] S. Vijayalakshmi et al., "Multi-perspective structural integrity-based computational investigations on airframe of Gyrodyne-configured multi-rotor UAV through coupled CFD and FEA approaches for various lightweight sandwich composites and alloys," Reviews on Advanced Materials Science, vol. 62, no. 1, pp. 1–49, Jan. 2023, doi: 10.1515/rams-2023-0147.

[13] K. Marangi and S. M. Salim, "Predicting the Structural Performance of the Wings of an Unmanned Aircraft Vehicle Using Fluid-structure Interaction," in Proceedings of the World Congress on Engineering 2019, 2019, pp. 1–6.

[14] R. Poletti, M. Barucca, L. Koloszar, M. A. Mendez, and J. Degroote, "DEVELOPMENT OF AN FSI ENVIRONMENT FOR THE AERODYNAMIC PERFORMANCE ASSESSMENT OF FLAPPING WINGS," in International Conference on Computational Methods for Coupled Problems in Science and Engineering, 2023, pp. 1–12.

[15] J. BLAZEK, Computational fluid dynamics principles and applications, 3rd ed. Oxford OX5: Elsevier, 2015.

[16] M. Ezkurra et al., "Analysis of One-Way and Two-Way FSI Approaches to Characterise the Flow Regime and the Mechanical Behaviour during Closing Manoeuvring Operation of a Butterfly Valve," International Journal of Mechanical and Materials Engineering, vol. 12, no. 4, pp. 409–415, 2018, [Online]. Available: https://www.researchgate.net/publication/325170283

[17] D. L. Logan, A First Course in the Finite Element Method, 6th ed. Boston: Cengage, 2023.

[18] S. Moaveni, Finite Element Analysis Theory and Applications with ANSYS, 4th ed. Essex: Pearson Education Limited, 2014. doi: 10.1016/0010-4485(84)90036-8.

[19] R. F. Gibson, PRINCIPLES OF MECHANICS MATERIAL COMPOSITE, 4th ed. Ohio: Taylor & Francis Group, LLC, 2016.

[20] M. Bhong et al., "Review of composite materials and applications," Mater Today Proc, no. June, 2023, doi: 10.1016/j.matpr.2023.10.026.

[21] Budynas Richard G. and Nisbett J. Keith, Shigley's Mechanical Engineering Design, 11th ed. New York: Mc Hall Eduication, 2020. [Online]. Available: http://www.elsevier.com/locate/scp

[22] M. I. Ali and J. Anjaneyulu, "Effect of fiber-matrix volume fraction and fiber orientation on the design of composite suspension system," in IOP Conference Series: Materials Science and Engineering, 2018, p. 012104. doi: 10.1088/1757-899X/455/1/012104.

[23] N. F. Saari et al., "Estimating natural frequency of pipe with various geometries: Improvement of

frequency factors," Heliyon, vol. 10, no. 4, p. e26148, 2024, doi: 10.1016/j.heliyon.2024.e26148.

[24] Z. Siddiqi and J. W. Lee, "A computational fluid dynamics investigation of subsonic wing designs for unmanned aerial vehicle application," Proc Inst Mech Eng G J Aerosp Eng, vol. June 2019, no. June 2019, pp. 1–10, 2019, doi: 10.1177/0954410019852553.

[25] A. Khaliq, M. A. Kamran, and M. Y. Jeong, "Nanoimprint Mold Consisting of an Adhesive Lap Joint between a Nanopatterned Metal Sleeve and a Carbon Composite Roll Amin," Nanomaterials, vol. 13, no. 10, pp. 1–14, 2023, doi: 10.3390/nano13101685.

[26] C. 2018 EDUPACK, "Epoxy/S-glass fiber, UD prepreg, QI lay-up," 2019. [Online]. Available: https://www.researchgate.net/profile/Janos-Plocher/post/Does_increasing_glass_fiber_weight_percentage_volume_fraction_increase_Modulus_in_GFRP_compsoitres/attachment/5c1cdb4dcfe4a764550a8b6d/AS%3A706252061564928%401545395021690/download/MaterialData~Epoxy